

Article

Seismic Upgrade of Steel Frame Buildings by Using Damped Braces

Eleonora Bruschi , Virginio Quaglini *  and Luca Zoccolini 

Department of Architecture, Built Environment and Construction Engineering, Politecnico di Milano,
Piazza Leonardo da Vinci 32, 20133 Milan, Italy

* Correspondence: virginio.quaglini@polimi.it; Tel.: +39-02-23994248

Abstract: Supplementary energy dissipation has proved to be an effective way of protecting structures from the disastrous effects of earthquakes and has been used in the last decades both in new and in existing constructions. In this regard, various procedures for the design of the damping system for the seismic retrofit of buildings have been formulated over the years, mainly focused on reinforced concrete (RC) constructions, which represent the largest part of the existing stock in many seismic-prone countries. The study deals with the assessment of a displacement-based design procedure for proportioning the damping system recently proposed in the literature for RC framed buildings, with the goal of establishing a good practice for the application of the procedure to steel buildings as well. The method was applied to three case-study frames, regular in plan and in elevation, which were assumed as being representative of old structures designed without consideration of seismic requirements. The retrofit was performed by using chevron braces equipped with dampers with an elastic-perfectly plastic behavior. The method aimed at defining the properties of the dampers to achieve a target performance in terms of the maximum lateral deflection for a specific level of seismic intensity. The effectiveness and reliability of the proposed procedure was eventually assessed by evaluating the seismic performance of the upgraded steel structures in static and dynamic non-linear analyses.

Keywords: energy dissipation; steel frame; seismic rehabilitation; damped braces; non-linear analyses; hysteretic dampers; buckling; OpenSees



Citation: Bruschi, E.; Quaglini, V.; Zoccolini, L. Seismic Upgrade of Steel Frame Buildings by Using Damped Braces. *Appl. Sci.* **2023**, *13*, 2063. <https://doi.org/10.3390/app13042063>

Academic Editor: Maria Favvata

Received: 8 December 2022

Revised: 1 February 2023

Accepted: 3 February 2023

Published: 5 February 2023



Copyright: © 2023 by the authors. Licensee MDPI, Basel, Switzerland. This article is an open access article distributed under the terms and conditions of the Creative Commons Attribution (CC BY) license (<https://creativecommons.org/licenses/by/4.0/>).

1. Introduction

A major issue in seismically prone countries is the vulnerability of the building heritage to earthquakes. Considering the European scenario, the largest part of the building stock, built before the 1980s of the last century, was designed according to outdated codes to withstand gravitational loads only [1]. Italy, Greece and Romania are the European countries with the highest seismic risk and reinforced concrete (RC) frame structures are among the most recurrent typologies in these regions [1]. For this reason, seismic upgrading of RC buildings has emerged as a main research area [2–5], and in recent years a number of technologies and design procedures have been investigated for the retrofit of RC structures, including the use of supplementary energy dissipation systems [6–16].

However, also steel structures designed before the publication of modern regulations (e.g., AISC 341-16 [17], ASCE 7-16 [18], EN 1993-1-1 [19], EN 1998-1 [20]) have been reported to suffer local and global collapses as a consequence of earthquakes [21–27]. Braces equipped with energy dissipation devices have proved to be effective in reducing the seismic demand for both RC [6–12,15] and steel structures [26–39], and the most updated codes (e.g., [17,18,20]) have incorporated general guidelines for the design of dissipative braces in new constructions, with the goals of limiting the lateral displacement and dissipating most of the seismic energy in auxiliary devices, avoiding any damage to the gravity-load resistant system [33,39–42].

Most of the procedures proposed in the literature [6–11,39,43–45] for dimensioning dissipative braces are based on the Direct Displacement-Based Design (DDBD) method [45], in which a “substitute” single degree of freedom (SDOF) model is used to replace the real multi-degree of freedom (MDOF) structure. The design of the dissipating system is performed to achieve, for a given seismic intensity level, a specified performance objective, expressed for example as a specific target displacement [11]. An extensive review of the most significant procedures developed for RC frames can be found in reference [11]. Kim and Seo [46] proposed a DDBD procedure for steel frames with non-moment-resisting joints supplemented with buckling-restrained braces (BRBs). The procedure neglects the column deformability and consequently it is applicable to low-rise buildings only. Ragni et al. [39] presented a simplified procedure for steel frames with pinned beam-to-column connections and dissipative braces equipped with either steel hysteretic devices or viscoelastic dampers. The procedure, which accounts for the deformability of both the braces and columns, is based on the formulation of a continuous cantilever model equivalent to the discrete bracing system and provides analytical expressions to distribute the flexural and shear stiffness of the diagonal braces and columns at each floor. In order to have a single parameter in the design procedure, only the first vibration mode of the equivalent continuous cantilever system is considered. While the above procedures deal with the design of new constructions, other researches focused on the retrofitting of steel moment-resisting frames (MRFs) [28,43,44] according to old regulations which have been found in need of seismic performance upgrade.

Some authors of this paper recently proposed a DDBD retrofit procedure [11,12,47,48], aimed at upgrading RC structures, regular in plan and in elevation, by means of dissipative braces. The procedure uses a recursive algorithm based on the Capacity Spectrum Method [49,50] to calculate the properties of the damped brace system, described by means of an equivalent SDOF system. Even if it has some analogies with other approaches based on the response spectrum and utilizing either the initial stiffness [7,9] or the secant stiffness to the maximum response level [6,10], the strength of the proposed method relies on its simplicity: the procedure requires to perform initially a pushover analysis to evaluate the capacity curve of the as-built structure, while in the subsequent steps the capacity curve of the retrofitted frame is calculated via simple analytical equations where the unknown parameter is the yield force of the equivalent damped brace. Analytical equations are also used to distribute the stiffness and strength properties of the dissipation braces at every floor of the real building with the target of matching the lateral deformation of the retrofitted frame to the first mode deformation of the as-built frame. This condition, which ensures the simultaneous engagement of the dampers at the different floors, is usually sought in all the design methods [10,34], because it maximizes the dissipation capacities of the system. The iterative procedure can be automated within a spreadsheet, resulting very convenient for professionals. Another attractive feature is that the procedure is code-compliant, since it has been formulated by taking into explicit account the provisions of the Italian Building Code (IBC) [51,52] and the Eurocode [53].

It is worth noting that the above method is very similar to the one developed independently for steel MRFs by Gutiérrez-Urzuá and Freddi [33], as both methods consist of a recursive procedure where the properties of an equivalent SDOF dissipation brace are defined by the comparison between the inelastic response spectrum demand and the capacity of the retrofitted frame in order to match a specified performance displacement. The main difference lies in the fact that the procedure by Bruschi and Quaglini [11], which has been formulated in compliance with IBC [51], represents the capacity curves of the equivalent SDOF frame which are used in the ADRS space for the application of the Capacity Spectrum Method by means of equivalent bilinear curves with post-yield hardening, in accordance with the recommendations of IBC’s Commentary [52].

The method [11] was applied in previous works to mid-rise residential RC buildings characterized by a fundamental period of about 1 s [11,12]. In comparison to RC buildings, steel structures are characterized by a substantially more flexible structural response, with

a non-negligible influence of P-delta effects, and a non-negligible column deformability especially in case of tall buildings, which can affect the vibration mode. The present study aims at assessing the viability of the retrofit procedure for steel MRFs and highlighting the possible limitations of the method. Three archetype configurations of MRFs with increasing number of floors (2, 4 and 8) affected by evident deficiencies such as non-equal bidirectional strength and stiffness in the main horizontal directions are considered [54,55]. The retrofit aims at upgrading the seismic performance of the buildings in order to comply with larger seismic demands, such as e.g., in cases of an update to the hazard maps and/or code regulations. For this purpose, the seismic hazard characteristics associated with the municipality of Lamezia Terme (seismic class 1 according to IBC [51], and soil type C) are considered.

The structure of the paper will follow this scheme. Chapter 2 provides fundamentals to the modeling choices adopted in the OpenSees framework for the non-linear behavior of steel members, with the further purpose of providing some useful indications to researchers who use this software program. The OpenSees software program (Open System for Earthquake Engineering Simulation) [56,57] has been indeed used since it facilitates the analysis of multi-story buildings in the non-linear regime with high accuracy and computational efficiency [58]. In Chapter 3, the three buildings selected as case studies are presented, while Chapter 4 details the modeling of the structures and of the dissipative bracing systems in OpenSees. The application of the retrofit design is explained in Chapter 5, and the results of the non-linear static and dynamic analyses (NLSAs and NLDAs) performed to verify the effectiveness and reliability of the procedure are shown in Chapter 6.

2. Modeling Approaches for Steel Structures in OpenSees

Non-linear analyses of steel structures fall into two main categories: distributed plasticity and concentrated (or lumped) plasticity analyses [58].

In the lumped plasticity approach [21,55,58–64], the beams and columns are modeled as elastic elements with plasticity concentrated in zero-length rotational springs at either ends. The zero-length rotational spring elements (implemented e.g., as *zeroLength* element object in the OpenSees framework [56,57]) generally include the modified Ibarra–Medina–Krawinkler (IMK) material model [65], which estimates the hysteretic behavior of beam–column connections capturing the strength degradation occurring both during monotonic loading after the strength cap is reached, and during consecutive cycles even though the strength cap has not been reached [54,64]. However, for MRFs, this model has been shown to have convergence issues in case of dynamic loading [58], due to high stiffness that must be assigned to the rotational springs in order to preserve the elastic stiffness of the beam. Moreover, the structural response is significantly affected by the selection of the damping model, and the Rayleigh damping model leads to unreliable results [66].

In contrast, the damping model has been demonstrated in several studies [67–70] to have less influence when the structural elements are formulated according to distributed plasticity models, such as e.g., fiber-based cross-section discretization [66]. According to the fiber-based cross-section discretization model, anelastic behavior can spread across the whole length of each element [60,67] and plastic hinges are activated at the most stressed sections when the yield limit is exceeded [58]. Another feature of this approach is that the influence of the axial force on the column moment-rotation relationship is directly taken into account [21], differently from the lumped plasticity model that requires each time to adjust the axial load-moment interaction based on the current axial load and moment gradient along the member [71]. Conversely, the lumped plasticity is more versatile than the distributed plasticity for simulating the cyclic degradation of strength and stiffness (low-cycle fatigue) [21], which has been demonstrated to significantly affect the seismic response of steel structures [58,72], especially in the event of long earthquakes [68]. In fact, mainly in the case of the I-shaped cross-sections, which are commonly used for the MRF beams, section deterioration begins in the sections subjected to the maximum moment, due to the triggering of flange local buckling in the compressed zone [73].

Since distributed plasticity models do not allow to incorporate explicitly the cyclic degradation, Bosco and Tirca [58] proposed a refined beam formulation, which is able to reproduce the strength and stiffness degradation of the I-shaped cross-sections and to replicate the failure mechanism caused by low-cycle fatigue. In particular, they formulated a fiber-based damage accumulation model by introducing a fatigue material wrapped around the uniaxial steel material used for the non-linear fiber section model assigned to the plastic hinges of the *beamWithHinges* element object [56,57]. In the *beamWithHinges* object, which can be used both for the beams and columns, the structural member is discretized into three sub-elements: a linear elastic material behavior is assigned to the internal sub-element while non-linear material behavior is associated with the two external sub-elements, whose length is assigned by the user. Different integration methods can be used with the *beamWithHinges* element object, varying with the number and location of the integration points [58]. In the proposal of Bosco and Tirca [58], the *beamWithHinges* element object was implemented with the modified Gauss–Radau integration scheme [57], and the uniaxial Giuffrè–Menegotto–Pinto constitutive law [74], corresponding to *Steel02* material model in the OpenSees framework [56,57], was assigned to each fiber of the plastic hinge zones. The low-cycle fatigue material was then combined with the *Steel02* material by implementing the *uniaxialMaterial Fatigue* element object [57], which uses an accumulative strain model to predict damage accumulation in accordance with the Miner’s rule. The fatigue material coefficients as well as the plastic hinge length (L_{pl}) of this model were calibrated by Bosco and Tirca [58] referring to a large number of experimental tests selected from the literature. The investigation eventually proposed (i) an equation to predict the variation of the fatigue ductility coefficient along the flange width, and (ii) an expression of the plastic hinge length L_{pl} for steel members in relation to the actual shear length L_v ($L_{pl} = 0.22 L_v$). This model proved to be effective especially when medium (~60 s) or long (~90 s) duration accelerograms are considered, as structural members are subjected to low-cycle fatigue, which affects the structural response [75]. On the contrary, for short durations of ground motion (less than 30 s), the degradation in stiffness and strength due to cumulated damage is not important [75].

3. Description of the Case-Study Frames

Three steel frame buildings, already used as case studies by other authors [54,55] and shown in Figures 1 and 2, are considered to apply the proposed methodology. The buildings consist of two-, four- and eight-story frames with a square plan ($24.0 \times 24.0 \text{ m}^2$), and three bays of 8.0 m each in the longitudinal and in the transversal main horizontal directions. The columns are continuous in elevation with an inter-story height of 4.0 m and oriented as shown in Figure 1. The beam sections correspond to IPE400 for each structure, while the column sections are HE400B, HE500B or HE600B according to Figure 2. The buildings, which have substantially different capacity along their two main horizontal directions due to the orientation of the cross-sections of the columns, are assumed as representative of old-code MRFs, designed without consideration of the requirement of similar resistance and stiffness characteristics in both main directions introduced in the current regulations [20]. Moreover, they envelope a wide range of fundamental periods of interest for conventional buildings [55].

S355 steel is used for the beams and columns, with yield and tensile strengths equal to 355 MPa and 510 MPa, respectively. As reported in reference [55], the structures were designed for low seismic hazard, corresponding to a design spectrum for soil A and peak ground acceleration (PGA) equal to 1.96 m/s^2 .

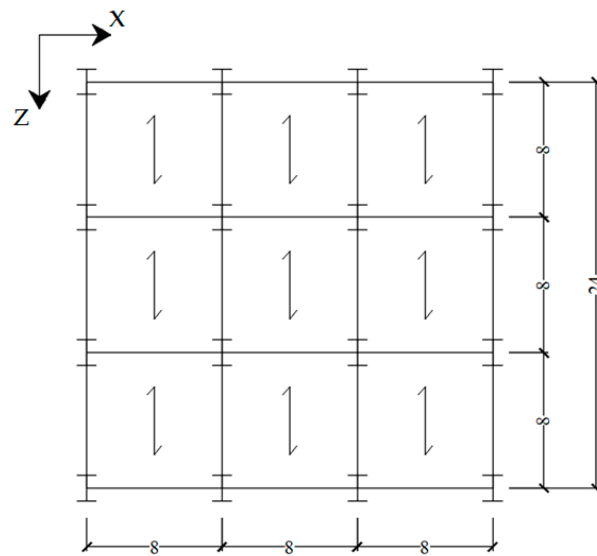


Figure 1. Typical plan of the three case-study structures (dimensions in m).

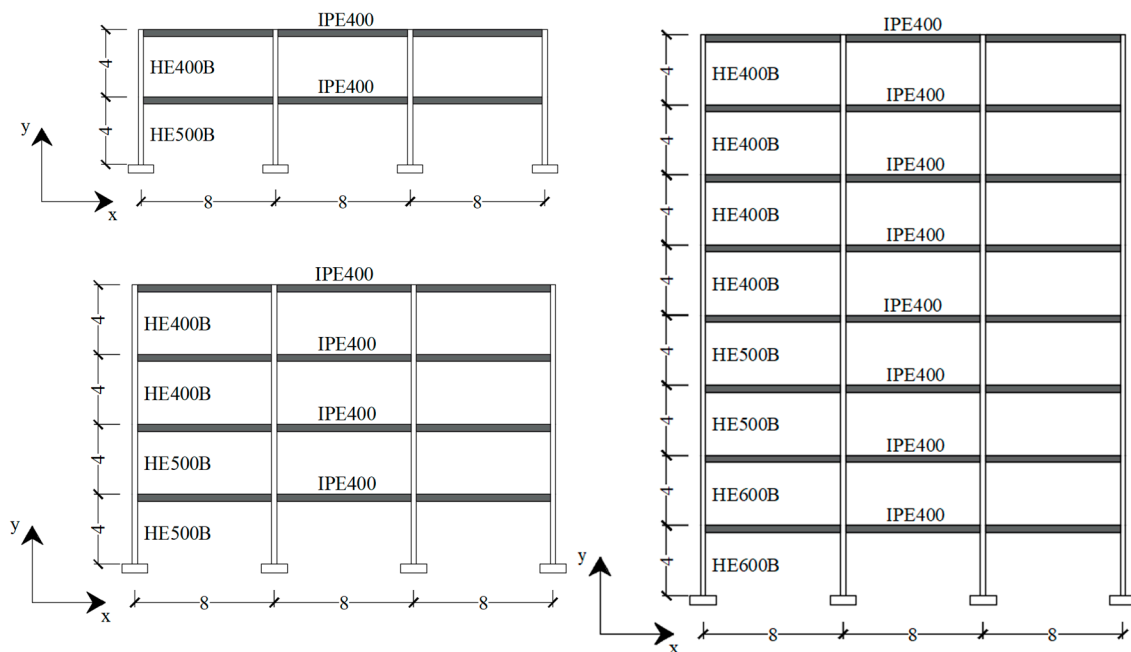


Figure 2. Elevation views of case-study structures (dimensions in m).

The assumed dead and live loads are reported in Table 1. The total live load Q includes 3 kN/m^2 live loads for use category B (offices) of the European [76] and Italian [51] design codes, and an additional 0.8 kN/m^2 contribution for movable partitions. Further information on design is reported in reference [55].

Table 1. Dead and live loads (n : number of stories; G : dead loads; Q : live loads).

Story	G [kN/m ²]	Q [kN/m ²]
1 to $n - 1$	4.11	3.80
n (roof)	3.74	3.80

4. Numerical Model in OpenSees

Fully 3D numerical models of the case-study structures were formulated using the OpenSees software program. The *forceBeamColumn* element object, in the form of the *beamWithHinges* element [57], was implemented for both beam and column members. A linear elastic material behavior was assigned to the internal sub-element of the *forceBeamColumn* object, while a fiber-based cross-section discretization was associated with the two external sub-elements. The length of these two sub-elements where inelastic behavior can be triggered was taken as $L_{pl} = 0.22 L_v$ according to references [58,75], where L_v is the shear length. The cyclic deterioration of the stiffness and strength of the structural members was disregarded as the bidirectional NLDAs were performed considering artificial ground motions characterized by a total duration of 25 s, as recommended in [51].

A two-point Gauss–Radau integration scheme for each sub-element was used in the element state determination, for a total of six integration points across the whole element object [71]. The cross-section of each external sub-element was discretized into 24 fibers, specifically eight fibers for each flange and eight fibers for the web [77–80]. The uniaxial Giuffrè–Menegotto–Pinto constitutive law [74], corresponding to the *Steel02* material model with isotropic strain hardening [81], was assigned to each fiber. The yield strength f_y , the modulus of elasticity E_s and the strain-hardening ratio b were taken equal to 355 MPa, 210,000 MPa and 0.01, respectively; the model parameters that control the transition from the elastic to the plastic branch were assumed as $R_0 = 18$, $C_{R1} = 0.925$ and $C_{R2} = 0.15$, consistently with reference [57].

The floor slabs were modeled as rigid diaphragms and the masses of the beams, columns and slabs were concentrated at the center of mass of each floor. The seismic masses at each floor were calculated according to code recommendations [51,76], taking a combination factor of 1.0 for the permanent loads and of 0.3 for the live loads as prescribed for use category B. The dead and live loads were calculated according to the tributary area concept and uniformly distributed on the beams along the X-direction (Figure 1). P-Delta effects were included in the analysis. The columns had fixed supports at the ground level, simulating rigid foundations. The structural damping of the frame was modeled as a function of the tangent stiffness matrix only, considering 3% on the first mode in line with references [82,83].

As in reference [55], the three MRFs were upgraded considering the seismic loads defined in the IBC [51] for life-safety limit state (SLV), in the municipality of Lamezia Terme (latitude 38.57°, longitude 16.18°), for functional class $c_u = 2$, nominal life $V_n = 100$, $PGA = 4.47 \text{ m/s}^2$, soil type C and topographic factor T_1 . The seismic retrofit of the structures is performed by means of steel braces equipped with steel hysteretic devices and arranged in a chevron (or “reversed V”) brace configuration. Such a configuration was adopted because it provides a direct relationship between the axial deflection of the damper and the structural inter-story drift [55,84,85]; nevertheless, alternative configurations can be implemented in the model as well. The braces are modeled as truss elements [57] associated with an *uniaxialMaterial* model with elastic behavior. The damper, placed at the intersection of the two braces and connected to the midsection of the beam, is modeled by a *zeroLength* element object [57] associated with an *uniaxialMaterial* model with elastic-perfectly plastic behavior [56,57], as commonly assumed in literature for hysteretic dampers [2,9,11,12,47,55].

5. Design of the Seismic Rehabilitation

The retrofit procedure [11,12,47,48] aims at proportioning the dissipating device(s) inserted in the braces in order to achieve the target structural performance. The procedure is iterative and consists of five steps.

5.1. Step 1: Definition of the Main Frame Capacity Curve

The capacity curve of the as-built structure ($V_F - d_F$) was determined via NLSAs as recommended in IBC [51]. The NLSAs were performed in the positive and in the negative X-

and Z- directions of the structure (Figure 1), by applying two horizontal force distributions proportional to either mass (UNIFORM distribution) or modal (MODAL distribution) properties (Figure 3), and considering 5% accidental eccentricity of the center of mass of each story. The $V_F - d_F$ capacity curve of the MDOF structure was then converted to the $V_F^* - d_F^*$ capacity curve of the equivalent SDOF system through the modal participation factor Γ , as shown in Figure 3.

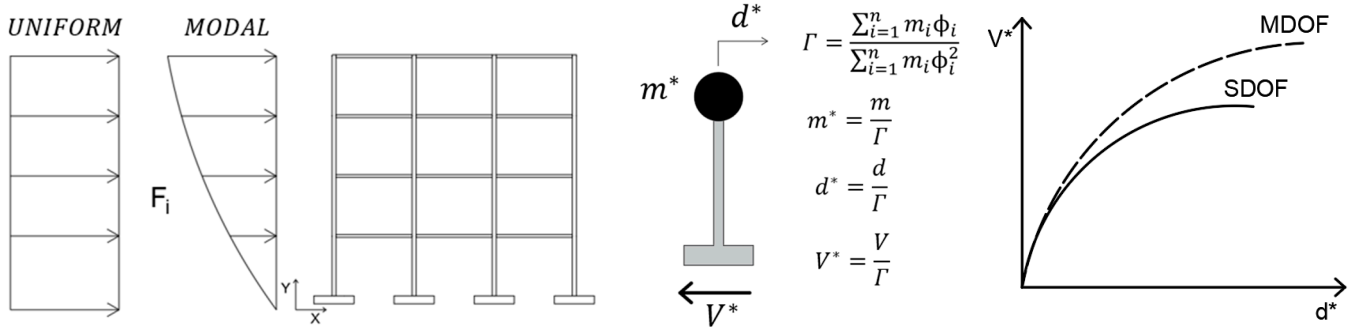


Figure 3. Determination of main frame capacity curves according to IBC.

In each of the two main horizontal directions, the lowest capacity curve was used to evaluate the properties of the equivalent SDOF system. As shown in Figure 4, for each MRF, there is a substantial difference between the capacity curves in X- and Z-directions, due to the preferred orientation of the cross-sections of the columns, which have their strong direction aligned to the Z-axis.

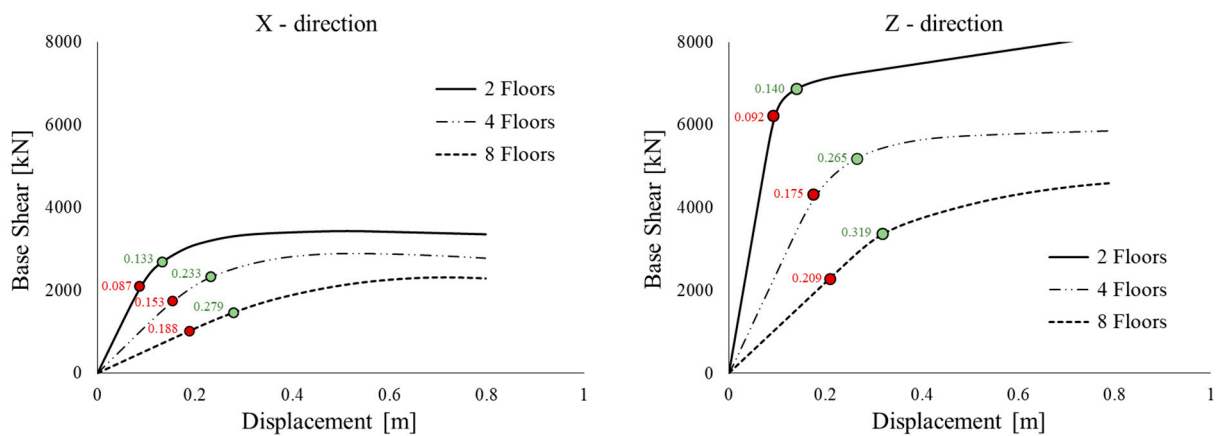


Figure 4. MODAL capacity curves of the as-built structures (MDOF) with indications of the target displacement d_p (green dots) and the yield displacement d_y (red dots).

5.2. Step 2: Definition of the Target Displacement and Construction of the Equivalent Bilinear Capacity Curve of the Main Frame

The target displacement d_p was defined based on the assumed building performance criteria, such as the story drift limits for the non-structural components or the plastic deformation limits for the structural members [39,86,87]. In agreement with reference [88], the immediate occupancy structural performance level, i.e., the condition in which the structure is immediately accessible as it retains its original strength and stiffness, was defined by the ending point of the elastic branch on the pushover curve. In the present case, the target displacement d_p was defined by multiplying the yield displacement d_y , identified as the limit of the elastic branch on the capacity curve [88] (Figure 4), by a ductility factor $\mu_F = 1.5$, in accordance with reference [55]. The choice of a ductility factor of 1.5, which involves a partial engagement of the main frame in the dissipation of the seismic energy, corresponded to the design strategy of relatively small dissipation braces, requiring minor

local strengthening requirements, while it limited at the same time the local damage of the structure after a strong earthquake.

The equivalent bilinear curve of the SDOF main frame was evaluated consistently with IBC [51] and clause C.7.3.4.2 of the Commentary [52] by respecting three conditions: (i) having the same initial stiffness as the continuous SDOF capacity curve, (ii) passing through the performance point of coordinates (d_p^*, V_p^{*F}) , and (iii) providing equivalence of areas A1 and A2 as shown in Figure 5. The equivalent SDOF system was characterized by an effective secant stiffness K_F^* , an effective period T_F^* and an equivalent viscous damping ratio ζ_F (in percent) defined again in Figure 5. The first term in the expression of ζ_F represents the contribution of the inelastic deformation of the frame to the total equivalent damping ratio, while the second term is the 3% inherent viscous damping assumed for steel structures [82,83]. The parameter κ_F was introduced to account for the energy dissipation capacity of the steel frame; it can be taken as 1.0 for high damping capability, 0.66 for moderate damping capability, and 0.33 for low damping capability [49]; in this study, κ_F is assumed equal to 1.

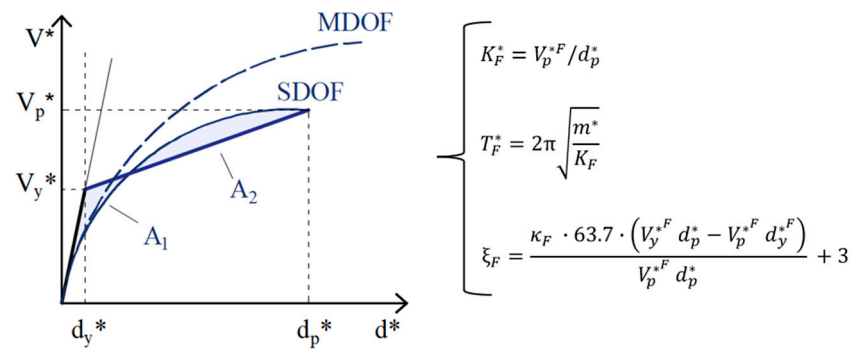


Figure 5. Determination of the equivalent bilinear curve of the main frame according to the Commentary of IBC.

Table 2 reports the properties of the equivalent SDOF systems of the case-study MRFs in their main horizontal directions.

Table 2. Properties of the equivalent SDOF systems of case-study MRFs.

Case-Study MRF	Direction	Γ [-]	m^* [ton]	d_y^{*F} [m]	V_y^{*F} [kN]	d_p^{*F} [m]	V_p^{*F} [kN]	ζ_F [%]
two-story	X	1.22	523.4	0.072	1729.0	0.109	2210.8	8.11
	Z	1.22	523.4	0.076	5085.2	0.0115	5616.6	15.77
four-story	X	1.27	1019.9	0.120	1380.7	0.183	1824.6	6.43
	Z	1.31	994.22	0.134	3306.6	0.203	3967.0	10.94
eight-story	X	1.29	2046.55	0.146	793.9	0.217	1141.0	1.48
	Z	1.31	2011.13	0.160	1750.4	0.244	2572.6	1.62

5.3. Step 3: Performance Check of the Main Frame

At step 3, the equivalent SDOF bilinear capacity curve $V_F^* - d_F^*$ was converted to the spectral coordinate $S_a = V_F^* / m^*$ (acceleration in m/s^2) and $S_d = d_F^*$ (displacement in m) and directly compared to the design response spectrum in the ADRS (Acceleration-Displacement Response Spectra) space.

In the ADRS space, the straight line from the origin through the point of coordinates $(d_F^*; V_F^* / m^*)$ has a slope $(2\pi / T_F^*)^2$ where T_F^* is the effective period of the equivalent SDOF frame defined in Figure 5. This line crosses the damped response spectrum relevant to the structural damping ζ_F at the point with spectral displacement $d_e^1 = S_d(T_F^*; \zeta_F)$. If $d_e^1 \leq d_p^*$, the as-built structure fulfills the performance requirement. On the other hand, if $d_e^1 > d_p^*$, the structure must be retrofitted in order to achieve the target performance.

Figure 6 shows, as an example, the comparison between the equivalent bilinear capacity curves of the four-story structure in the X- and Z- directions and the relevant demand response spectra. As evident, in the Z-direction the main frame meets the target performance; instead, in the X-direction, retrofit is necessary to control the lateral deformation. Same results were obtained for the two-story structure; on the contrary, for the eight-story, MRF retrofit is required in both the X- and Z-directions. For sake of brevity, only the results relevant to the four-story frame are shown.

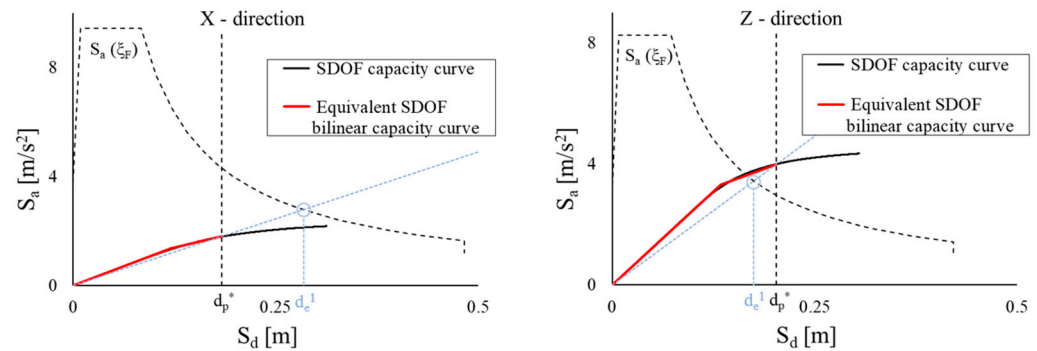


Figure 6. Comparison of the equivalent SDOF bilinear capacity curves of the four-story frame with the relevant demand response spectra in X- and Z-directions.

5.4. Step 4: Determination of the Equivalent Damped Brace System

In this work, hysteretic dampers with an elastic-perfectly plastic behavior similar to those assumed in other studies [2,9,11,12,47,55] were considered. Figure 7 shows the force-displacement curve of the equivalent SDOF damped brace, modeled as an in-parallel system of an elastic steel brace (B) and an equivalent SDOF hysteretic damper (D). The equivalent damping of the system ζ_{DB} was calculated according to the formula reported in Figure 7, where κ_{DB} is a parameter that accounts for the energy dissipation capacity of the damper and is calibrated on experimental tests [12,48].

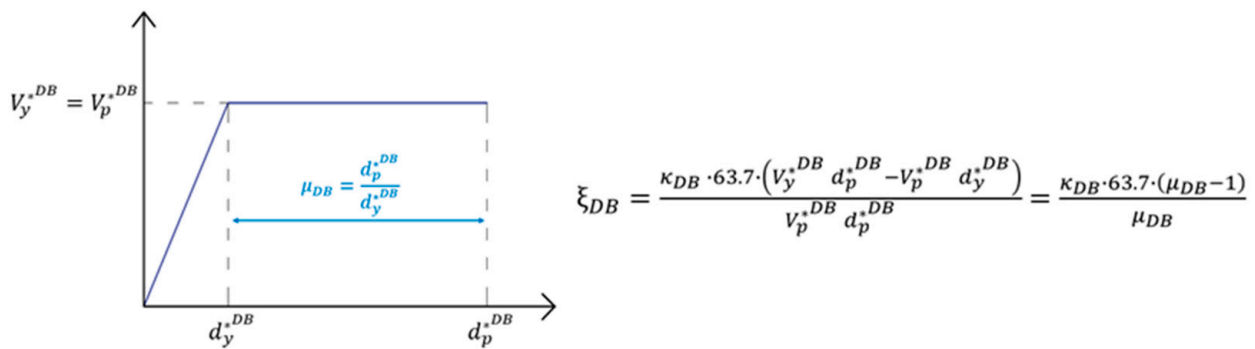


Figure 7. Force-displacement of the equivalent SDOF damped brace. V_y^{*DB} and V_p^{*DB} : yield and ultimate force; d_y^{*DB} and d_p^{*DB} : yield and ultimate displacement; μ_{DB} : ductility factor.

The ductility μ_{DB} of the dampers was chosen at the beginning of the retrofit procedure by the designer, considering the characteristics of the devices available on the market. For steel hysteretic dampers, μ_{DB} is typically between 4 and 10, providing an equivalent viscous damping ratio between 20 and 40% [9,10,39,89]. In this study, two analyses were performed considering the two boundaries of the range, namely $\mu_{DB} = 4$ and $\mu_{DB} = 10$ [11].

At the first iteration of the procedure, the effective viscous damping ratio ζ_{eff}^1 of the combined in-parallel system (F + DB) made of the equivalent SDOF frame and the equivalent SDOF damped brace was evaluated in order to fulfill the displacement equality $S_d(T_F^*; \zeta_{eff}^1) = d_p^*$. By evoking the damping correction factor according to [20],

$S_d(T_F^*, \zeta_{eff}^1) = S_d(T_F^*, \zeta = 3\%) \cdot \sqrt{\frac{10}{5 + \zeta_{eff}^1}}$, leading to $\zeta_{eff}^1 = 10 \cdot \left(\frac{S_d(T_F^*, \zeta = 3\%)}{d_p^*} \right)^2 - 5$. Eventually, ζ_{eff}^1 can be expressed according to the energetic equivalence of Equation (1), where the yield force $V_{p,1}^{*DB}$ of the damped bracing system is the unknown.

$$\zeta_{eff}^1 \cdot V_p^{*F} = \zeta_F \cdot V_p^{*F} + \zeta_{DB} \cdot V_{p,1}^{*DB} \tag{1}$$

Once $V_{p,1}^{*DB}$ was determined from Equation (1), the equivalent bilinear curve of the equivalent SDOF retrofitted frame (F + DB) was constructed and plotted in the ADRS space, Figure 8. The ultimate displacement of the capacity curve of the braced frame is equal again to the target displacement d_p^* , while the corresponding force at second iteration becomes $V_{p,2}^{*F+DB} = V_p^{*F} + V_{p,1}^{*DB}$.

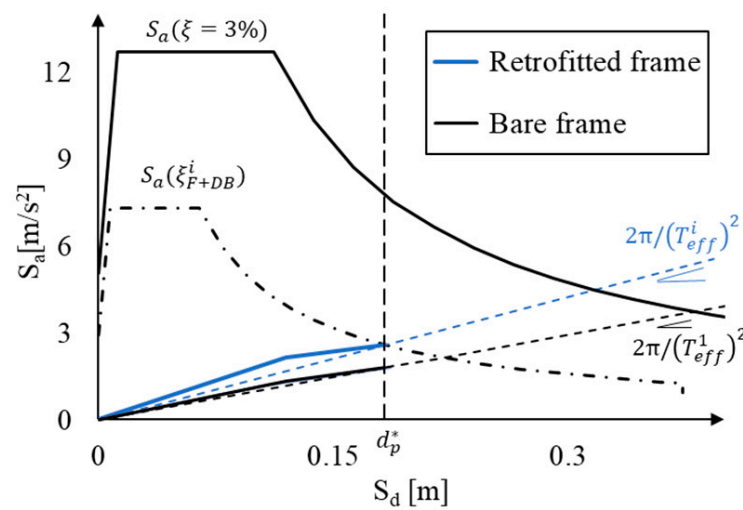


Figure 8. Graphical representation of the iteration of Step 4 for evaluating the properties of the equivalent SDOF damped brace.

Step 4 was iterated until the displacement at the performance point of the equivalent SDOF braced frame (F + DB) converges to the target displacement d_p^* . At the i^{th} iteration, the equivalent damping ratio of the retrofitted frame ζ_{eff}^i is expressed by Equation (2) where $V_{p,i}^{*DB} = V_{y,i}^{*DB}$ is the only unknown, as $V_{p,(i-1)}^{*DB}$ has been determined in the previous iteration.

$$\zeta_{eff}^i \cdot (V_p^{*F} + V_{p,(i-1)}^{*DB}) = \zeta_F \cdot V_p^{*F} + \zeta_{DB} \cdot V_{p,i}^{*DB} \tag{2}$$

As shown in Figure 8, the graphical representation in the ADRS plane shows at each iteration the relationship between demand and capacity. It must be noted that, at the i^{th} iteration, the effective stiffness and the effective period of the equivalent SDOF upgraded frame are equal to $K_{F+DB}^i = (V_p^{*F} + V_{p,i}^{*DB}) / d_p^*$, and $T_{eff}^i = 2\pi \sqrt{\frac{m^*}{K_{F+DB}^i}}$, respectively.

For the three case-study MRFs, the convergence was reached at the third iteration. The properties of the equivalent SDOF damped braces are finally reported in Table 3.

Table 3. Properties of the equivalent SDOF damped braces (d_y^{*DB} yield displacement; d_p^{*DB} ultimate displacement equal to the MRF target displacement d_p^* ; $V_p^{*DB} = V_y^{*DB}$ ultimate and yield force; $K_y^{DB} = V_y^{*DB} / d_y^{*DB}$ elastic stiffness; $K^{DB} = V_p^{*DB} / d_p^{*DB}$ effective stiffness).

Case-Study MRF	Direction	μ_{DB}	d_y^{*DB} [m]	d_p^{*DB} [m]	$V_p^{*DB} = V_y^{*DB}$ [kN]	K_y^{DB} [kN/mm]	K^{DB} [kN/mm]	
Two-story	X	4	0.027	0.11	588.93	21.57	5.39	
		10	0.011	0.11	503.50	46.10	4.61	
Four-story	X	4	0.046	0.18	951.52	20.80	5.20	
		10	0.018	0.18	810.93	44.32	4.43	
Eight-story	X	4	0.054	0.22	2212.45	40.77	10.19	
			Z	0.061	0.24	1657.90	27.15	6.79
	Z	10	X	0.022	0.22	1888.77	87.01	8.70
			Z	0.024	0.24	1413.71	57.87	5.79

5.5. Step 5: Distribution of the Damped Braces across the Frame

The distribution of the elastic stiffness and yield force of the dissipative braces at each floor of the real structure was performed according to a proportionality criterion [7,8,38] with the goal of matching the modal shape of the retrofitted frame to the first mode shape of the as-built frame. For this reason, the regularity of the frame in plan and in elevation was considered as a fundamental prerequisite for the application of this method. This solution aims at producing the simultaneous yielding of the dissipative devices at all the stories, and thus a global ductility of the damping system coinciding with the ductility of the single dampers. Such condition on one hand legitimates the condensation of the properties of the damping system into an equivalent SDOF device assumed in the design procedure, and in addition maximizes the energy dissipation capacity [33,34].

At each floor, the properties of the damped braces were evaluated by applying the formulas shown in Figure 9, where ϕ_i is the i -th component of the first mode eigenvector of the main frame, N_{yi}^{DB} and K_{yi}^{DB} are the yield force and the elastic stiffness of the single damped brace at the i th floor and n_d is the total number of dampers per floor. Eventually the stiffness of the steel braces and the properties of the dampers were calculated based on geometrical considerations depending on the particular brace arrangement.

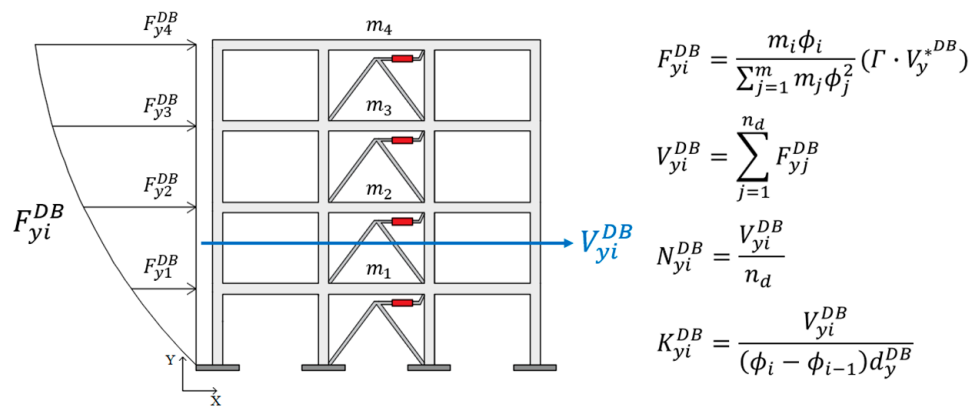


Figure 9. Graphical representation of the procedure for distributing the properties of the damped braces at the stories of the frame.

In the present work, steel hysteretic dampers were inserted within a chevron brace in the perimetral bays of the MRFs according to the plan layout shown in Figure 10. In the two-story and four-story structures, the dampers were inserted in X-direction only (Figure 10a), with two dampers per story, while the eight-story frame was upgraded in both horizontal directions (Figure 10b). Each damped brace (DB) was composed of an

in-series arrangement of a damper (D) and two inclined steel braces (B) according to the typical chevron brace configuration. Therefore, the lateral deformation of each story was accommodated by the deflections of both the damper and the braces in proportion to their stiffnesses. In order to concentrate almost the whole deformation of the story in the damper [90] and increase the amount of energy dissipation, the stiffness of the chevron braces K_i^B is set equal to fifteen times the effective stiffness of the damper K_i^D , in accordance with other studies [31,91]. It must be observed that, while such an assumption is fully realistic for the two-story and the four-story buildings, it provides, for the braces installed at the first floors of the eight-story frame, dimensions that could become economically not practicable though technically feasible. Nevertheless, in this study, it was decided to adopt the same figure of the stiffness ratio also for the eight-story MRF in order to maintain a coherent strategy for all the case studies. In a practical application, obviously the designer will have to verify case by case the convenient value of the stiffness to be adopted, taking into account the resulting dimensions of the braces. The identified properties (elastic stiffness and yield force) of the dampers at each floor are reported in Tables 4–6. The effective stiffness of the single damper K_i^D is simply calculated by dividing the elastic stiffness by the relevant damping factor.

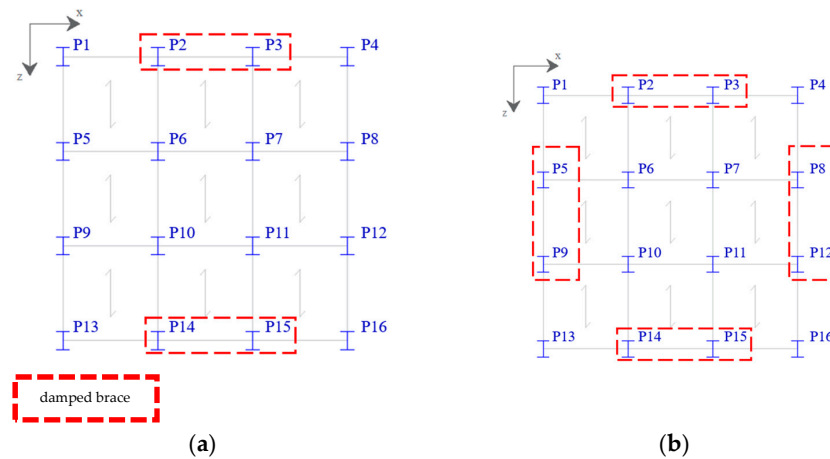


Figure 10. Plan layout of damped braces in (a) two-story and four-story structures, (b) eight-story structure.

Table 4. Two-story MRF: elastic stiffness K_{yi}^D and yield force N_{yi}^D of the dampers at each story in X-direction for $\mu_{DB} = 4$ and $\mu_{DB} = 10$.

Story	$\mu_{DB} = 4$		$\mu_{DB} = 10$	
	K_{yi}^D [kN/mm]	N_{yi}^D [kN]	K_{yi}^D [kN/mm]	N_{yi}^D [kN]
2nd	29.5	232.7	63.1	199.0
1st	46.7	357.9	99.7	306.0

Table 5. Four-story MRF: elastic stiffness K_{yi}^D and yield force N_{yi}^D of the dampers at each story in X-direction for $\mu_{DB} = 4$ and $\mu_{DB} = 10$.

Story	$\mu_{DB} = 4$		$\mu_{DB} = 10$	
	K_{yi}^D [kN/mm]	N_{yi}^D [kN]	K_{yi}^D [kN/mm]	N_{yi}^D [kN]
4th	52.5	214.1	111.9	182.5
3rd	55.4	412.3	118.0	351.4
2nd	61.3	547.5	130.6	466.6
1st	88.2	606.4	187.9	516.8

Table 6. Eight-story MRF: elastic stiffness K_{yi}^D and yield force N_{yi}^D of the dampers at each story in X- and Z-directions for $\mu_{DB} = 4$ and $\mu_{DB} = 10$.

Story	X-Direction				Z-Direction			
	$\mu_{DB} = 4$		$\mu_{DB} = 10$		$\mu_{DB} = 4$		$\mu_{DB} = 10$	
	K_{yi}^D [kN/mm]	N_{yi}^D [kN]	K_{yi}^D [kN/mm]	N_{yi}^D [kN]	K_{yi}^D [kN/mm]	N_{yi}^D [kN]	K_{yi}^D [kN/mm]	N_{yi}^D [kN]
8th	282.2	370.0	602.3	315.9	139.8	290.2	298.0	247.4
7th	300.5	756.3	641.3	645.6	168.9	588.3	360.1	501.6
6th	302.6	1111.6	645.8	949.0	173.5	857.0	369.9	730.8
5th	303.7	1421.7	648.1	1213.7	175.2	1084.1	373.4	924.4
4th	325.3	1675.0	694.2	1429.9	193.7	1259.6	413.0	1074.1
3rd	327.8	1865.3	699.6	1592.4	213.5	1380.5	455.1	1177.2
2nd	349.0	1985.3	744.9	1694.9	274.1	1446.7	584.2	1233.6
1st	510.8	2034.9	1090.2	1737.2	585.5	1468.1	1248.2	1251.8

Some concluding remarks have to be made concerning the current limitations of the procedure.

First, it should be noted that the first part of the procedure relevant to the calculation of the lumped properties of the braced system (steps 1 to 4) is valid whether or not the main frame is regular, as it relies on an equivalent SDOF model of the real structure. The regularity of the frame in plan and in elevation is instead assumed as a prerequisite by the distribution criterion adopted in step 5. In the case of structures affected from vertical irregularities, a constant drift ratio criterion and a constant shear ratio criterion for the in-elevation distribution of the stiffness and strength, respectively, can be found in reference [8]. Second, the procedure, which was originally developed for the RC frames, disregards the axial deformability of the columns, which can be non-negligible in case of steel frames, especially in tall buildings. The axial deformability of the columns can indeed impair their flexural deformability and reduce the horizontal stiffness of the structure, inducing a significant effect on the vibration mode of the frame [92]. Additionally, the procedure relies on a “substitute” equivalent SDOF system and vibration modes higher than the first mode are neglected. These assumptions limit the validity of the proposed procedure to small- and medium-rise buildings.

6. Seismic Response Assessment

In order to investigate the effectiveness and reliability of the method, the NLSAs and NLDAs were performed on both as-built and retrofitted structures.

Figure 11 compares in the ADRS space the capacity curves in the X-direction of the three as-built MRFs (indicated as *Frame* in the Figure) to the curves of the upgraded structures with $\mu_{DB} = 4$ (red line) and $\mu_{DB} = 10$ (blue line). The target displacement is matched by the three upgraded frames for both values of μ_{DB} . As shown in the Figure, for the two-story and the four-story frames, the post-yield branches of the curves relevant to either μ_{DB} are practically overlapped; in contrast, though the design target is matched in both configurations, a non-negligible difference exists between the capacity curves of the eight-story structure.

The bidirectional NLDAs were performed according to the Italian [51] and European [20] codes, considering seven pairs of artificial ground motions generated by the computer code SIMQKE [93] and characterized by a duration of 25 s each [51]. The performance of the retrofitted frames was evaluated in terms of the maximum displacement (d_{max}) and the maximum acceleration (PFA) at each floor; moreover, the compressive axial force (N) in the columns due to the seismic loads was calculated to check if the buckling limitation defined by the IBC [51] was respected. The mean values of the maxima of these parameters for the seven pairs of bidirectional accelerograms are reported in Figures 12–14.

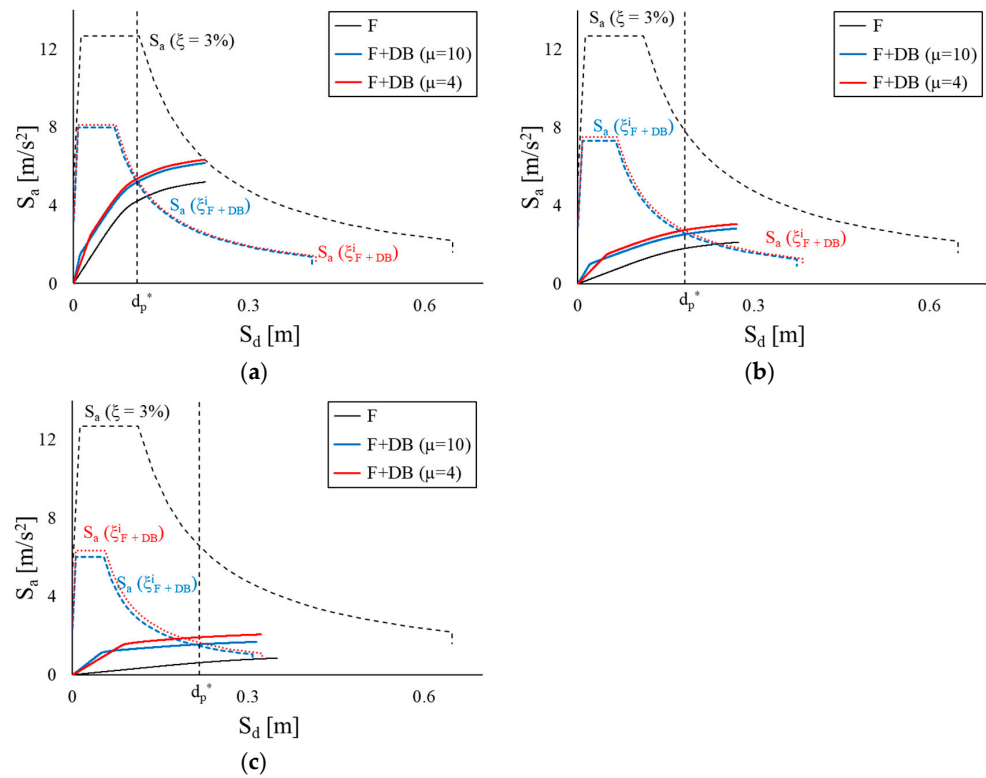


Figure 11. Results of NSLAs in X-direction of (a) two-story, (b) four-story, and (c) eight-story structures.

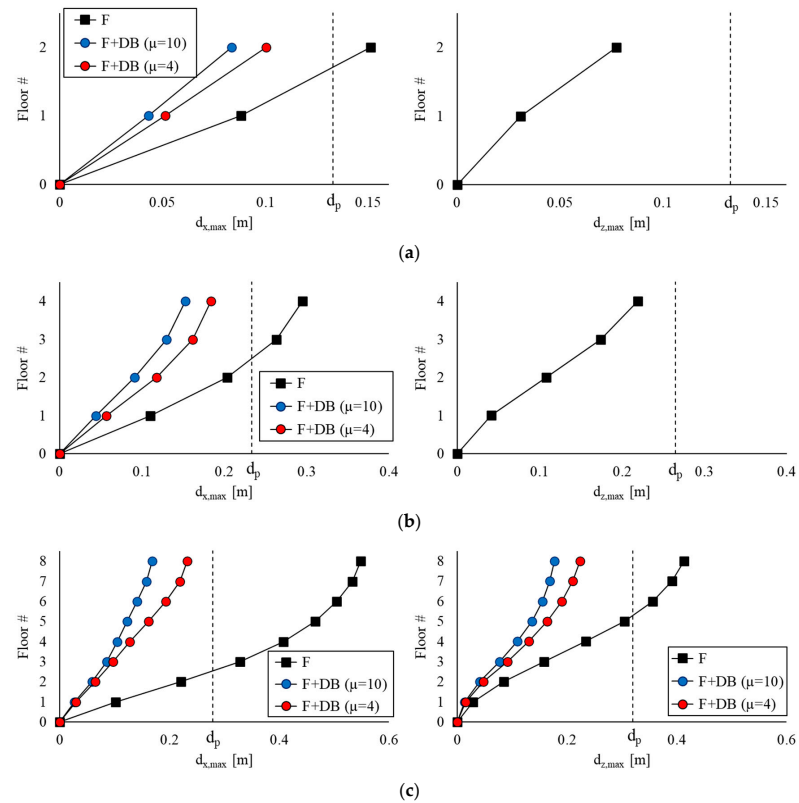


Figure 12. Maximum displacement at each floor of case-study MRFs with and w/o damped braces: (a) two-story, (b) four-story, and (c) eight-story structures.

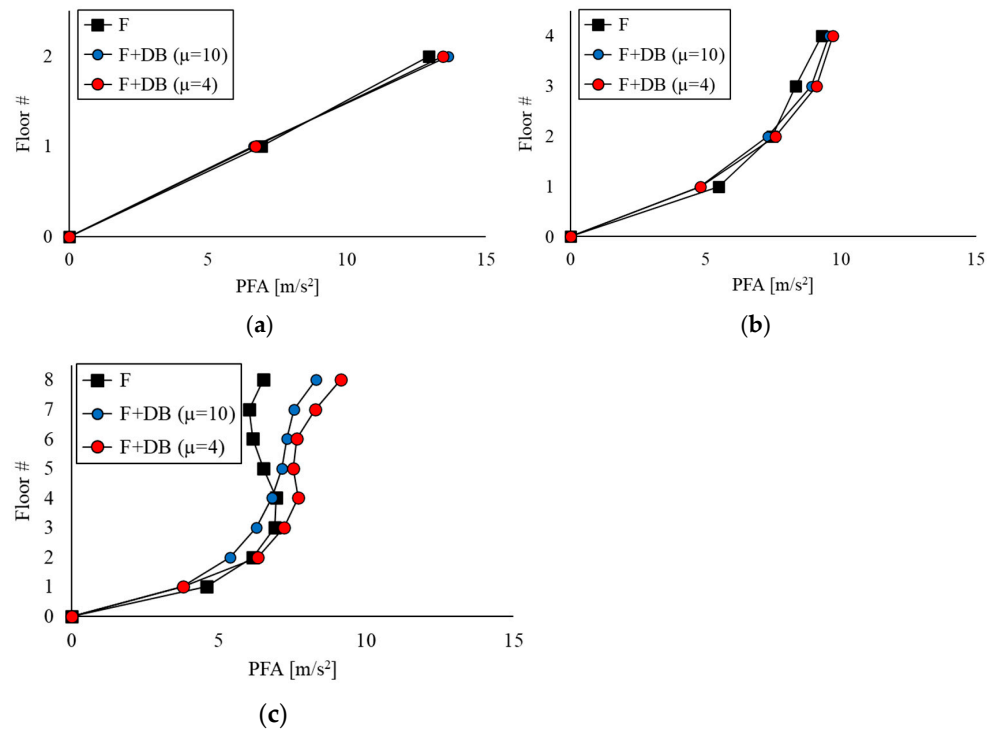


Figure 13. Peak Floor Acceleration of the case-study MRFs with and w/o damped braces: (a) two-story, (b) four-story, and (c) eight-story structures.

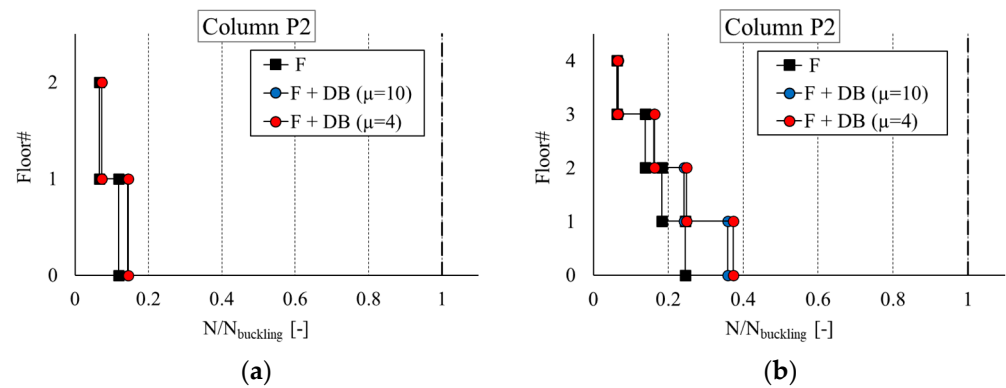


Figure 14. Buckling checks in the most stressed column in (a) two-story MRF and (b) four-story MRF.

Figure 12 shows the results in terms of the maximum displacement in the X- and Z-directions, indicated as $d_{x,max}$ and $d_{z,max}$, respectively. The introduction of the damped braces produced a significant decrease in the lateral displacement, below the design target. It is also worth noting that the upgraded MRFs exhibited similar stiffness in the two main horizontal directions, respecting the relevant requirement provided in EC8 [20]. On the other hand, the procedure was shown to provide conservative results, as the averaged roof displacement of all retrofitted buildings was smaller than the target displacement d_p : considering the three MRFs, the gap in the X-direction ranged between 17 and 25% with $\mu_{DB} = 4$ and between 35 and 45% with $\mu_{DB} = 10$, while in the Z-direction (8-story MRF only) the gap was about 30% with $\mu_{DB} = 4$ and 40% with $\mu_{DB} = 10$.

The tendency of the method to provide a conservative design of the damped brace system when checked against the NLDAs has been already highlighted and discussed in previous works [11,94]. This behavior can be explained by considering that the results of the NLSAs used to evaluate the capacity curve of the main frame at the beginning of the design procedure depend on the assumed distribution of lateral forces and neglect the dynamic

effects. Moreover, the design procedure accounts for the damping introduced from both the inelastic deformation of the main frame and the engagement of the dissipation system by modifying the response spectrum by the damping correction factor $\eta = \sqrt{10/(5 + \zeta_{F+DB})}$. However, owing to the large damping capability of the damped braces investigated in the study, the ensuing value of η is less than 55%, which is the threshold over which the reduced shapes of the pseudo-acceleration and displacement response spectra are no longer valid [53].

The maximum bidirectional peak floor acceleration (PFA) at each story is plotted in Figure 13. The two-story and four-story frames do not show a significant increase in the PFA moving from the bare to the upgraded configurations. In the eight-story structure, the PFA has a non-negligible increase, especially from the fifth up to the last floor, where the PFA passes from 6.5 m/s² in the bare configuration to 8.3 m/s² and 9.1 m/s² in the retrofitted configurations for $\mu_{DB} = 10$ and $\mu_{DB} = 4$, respectively.

The introduction of the damped braces in a frame causes an increment of the internal forces in the structural members adjacent to the upgraded bay. Therefore, the maximum compressive axial forces of the columns are evaluated at each floor and divided by the corresponding buckling load (N_{buckling}) calculated according to IBC [51], to check if the buckling capacity is exceeded. Figure 14 shows the check results for the most stressed element of the two-story and four-story MRFs (column P2 according to the layout in Figure 10a), highlighting that, for these structures, the buckling limitation requirement is satisfied. On the contrary, the most stressed elements of the eight-story MRF (columns P2 and P5 according to Figure 10b) do not respect the buckling limit at the first floor in the retrofitted configuration with $\mu_{DB} = 10$ and at both the first and second floors in the retrofitted configuration with $\mu_{DB} = 4$ (Figure 15a). In Z-direction, the buckling threshold is not respected only at the ground floor by column P5 in the retrofitted configuration with $\mu_{DB} = 4$, where N/N_{buckling} is equal to 1.025 (Figure 15b).

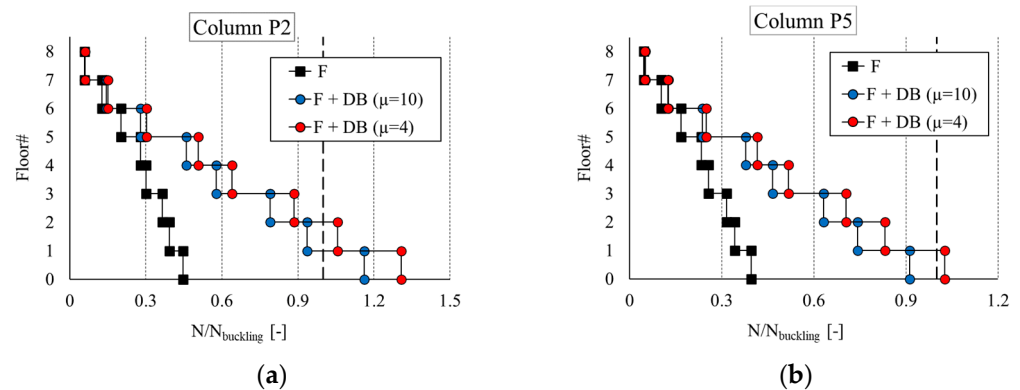


Figure 15. Buckling checks in the most stressed columns in the eight-story MRF: (a) column P2 and (b) column P5.

In order to fulfill the buckling limitations, the design of the chevron braces with the hysteretic devices is repeated for the eight-story structure by inserting two braces per each perimetral frame in the X-direction, as shown in Figure 16a; in the Z-direction, only one chevron brace per frame is kept. The properties of the devices in the new configuration with two dampers per frame are half of those calculated in the previous configuration. Figure 16b shows that with the new damper layout, the maximum values of the normalized axial force (N/N_{buckling}) for column P3, which results the most stressed element in the new retrofitted configuration for either μ_{DB} , are less than unity.

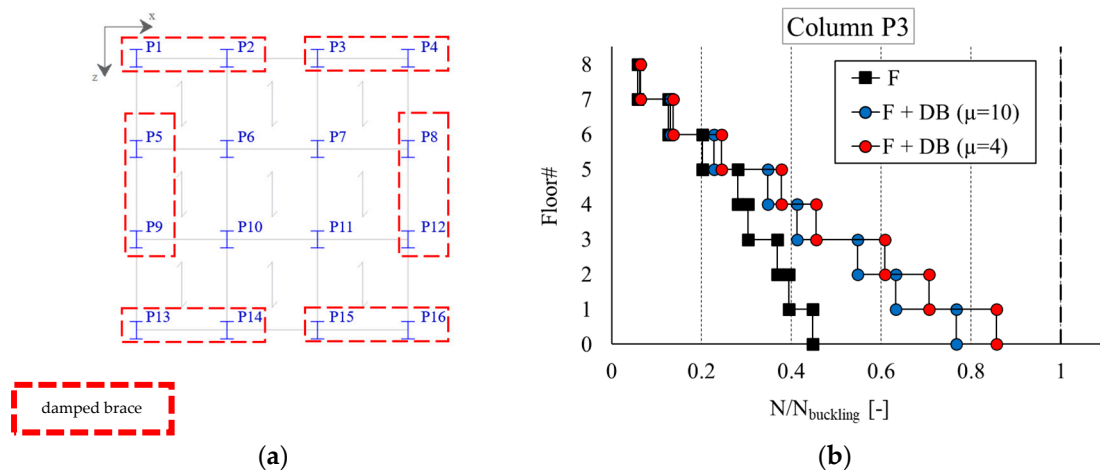


Figure 16. (a) new plan layout of damped braces in the eight-story MRF; (b) buckling checks in column P3 of the retrofitted frame.

Beyond the possible global collapse due to buckling, it must also be considered that the axial deformability of the columns, which is normally neglected in design due to the complexity of the analyses, can significantly reduce the horizontal stiffness of the moment-resisting frame and cause it to collapse in the presence of ground motions of high intensity. In fact, although code provisions tend to discourage yielding of the columns over the frame height using capacity design considerations, significant yielding may occur in the columns at ground level of the tall frames in the case of a major seismic event, causing to degrade the restoring force of the steel frame and leading to the potential formation of a single-story mechanism and eventually the dynamic collapse of the structure under strong earthquakes [31,95,96]. However, this aspect has not been covered in this study.

7. Conclusions

The study investigated the viability of a displacement-based design procedure, originally conceived for the RC structures, for dimensioning the hysteretic dampers for the seismic rehabilitation of steel frame buildings. The procedure is applicable to low- and mid-rise buildings with regular distribution of masses and stiffnesses in plan and in elevation, for which the dynamic response is essentially governed by the first mode. Three case-study moment-resisting frames of two, four and eight stories, unable to meet the seismic performance requirements according to the current codes, have been investigated and the seismic retrofit has been designed examining two damper solutions, characterized by high and low ductility values (10 and 4, respectively). Eventually, the effectiveness of the design was verified by means of the NLSAs and NLDs.

The main results of the study are summarized as follows.

- (1) The proposed procedure proved to be a viable means for proportioning the damped braces of the low- and mid-rise steel frames in order to achieve a target performance defined in terms of the maximum lateral displacement of the frame.
- (2) The design of an effective dissipation brace system for a steel frame must take into account also the ensuing increase in the internal forces of the structural members of the bays where the braces are introduced. For mid-rise buildings, an issue is represented by the increase in axial force and possible buckling of the columns for the seismic loads. For these buildings, it is recommended to explore different layouts for the brace system, especially at the lower stories.
- (3) In this study, two ductility factors, representing the upper and lower bounds for the conventional hysteretic dampers, were examined. For low-rise buildings, the performance of the upgraded structure was scarcely affected by the characteristic of

the dampers, while for the mid-rise frame a non-negligible influence of the ductility factor of the damper system was highlighted from the NLDAs.

- (4) The analyses showed that the design procedure is conservative, and that the structural displacement calculated via the NLDAs is significantly smaller than the design target; this difference tends to increase as the ductility of the dampers increases.
- (5) Even though more cases need to be examined to validate these outcomes, the study provides some guidance to professionals who have to tackle with the seismic upgrading of steel frames with damped brace systems, by illustrating a handy procedure for the design and dimensioning of the damper layout and giving some practical suggestions for the assessment of the overall structural response.

There are still some limitations in this study. Firstly, the procedure was applied to three archetypes of steel moment-resisting frames with an obvious non-symmetric distribution of strength and stiffness in the two main horizontal directions due to an unusual arrangement of column sections. Second, all the beam-to-column connections of the frame are moment resisting, which is a bit of an unusual approach according to the European practice. Finally, the procedure considers only structures that are regular in plan and in elevation.

The future research will focus on the application to real low-rise and mid-rise steel structures, as well as will explore the extension of the procedure to in-elevation irregular frames and unsymmetric-plan arrangements.

Author Contributions: Conceptualization, E.B. and V.Q.; methodology, E.B. and V.Q.; software, E.B. and L.Z.; supervision, V.Q.; validation, V.Q.; writing—original draft, E.B.; writing—review and editing, V.Q. All authors have read and agreed to the published version of the manuscript.

Funding: This work was funded by the Italian Department of Civil Protection (DPC) in the frame of the national Research Project DPC-ReLUIS 2022–2024, Work Package WP 15 “Contributi normativi a isolamento e dissipazione”.

Data Availability Statement: The data presented in this study are available on request from the corresponding author. The data are not publicly available as generated within research funded by the Italian Department of Civil Protection.

Conflicts of Interest: The authors declare no conflict of interest.

References

1. Landolfo, R.; Formisano, A.; Di Lorenzo, G.; Di Filippo, A. Classification of european building stock in technological and typological classes. *J. Build. Eng.* **2022**, *45*, e103482. [[CrossRef](#)]
2. Barbagallo, F.; Bosco, M.; Marino, E.M.; Rossi, P.P.; Stramondo, P. A multi-performance design method for seismic upgrading of existing RC frames by BRBs. *Earthq. Eng. Struct. Dyn.* **2017**, *46*, 1099–1119. [[CrossRef](#)]
3. Cao, X.Y.; Shen, D.; Feng, D.C.; Wang, C.L.; Qu, Z.; Wu, G. Seismic retrofitting of existing frame buildings through externally attached sub-structures: State of the art review and future perspectives. *J. Build. Eng.* **2022**, *57*, 104904. [[CrossRef](#)]
4. Cao, X.Y.; Feng, D.C.; Li, Y. Assessment of various seismic fragility analysis approaches for structures excited by non-stationary stochastic ground motions. *Mech. Syst. Signal. Process.* **2023**, *186*, 109838. [[CrossRef](#)]
5. Cao, X.Y.; Feng, D.C.; Wu, G.; Wang, Z. Experimental and theoretical investigations of the existing reinforced concrete frames retrofitted with the novel external SC-PBSPC BRBF sub-structures. *Eng. Struct.* **2022**, *256*, 113982. [[CrossRef](#)]
6. Bergami, A.V.; Nuti, C. A design procedure of dissipative braces for seismic upgrading structures. *Earthq. Struct.* **2013**, *4*, 85–105. [[CrossRef](#)]
7. Mazza, F.; Vulcano, A. Displacement-Based Design procedure of damped braces for the seismic retrofitting of RC framed buildings. *Bull. Earthq. Eng.* **2015**, *13*, 2121–2143. [[CrossRef](#)]
8. Mazza, F.; Mazza, M.; Vulcano, A. Displacement-Based seismic Design of hysteretic damped braces for retrofitting in-elevation irregular RC framed buildings. *Soil Dyn. Earthq. Eng.* **2015**, *69*, 115–124. [[CrossRef](#)]
9. Di Cesare, A.; Ponzio, F.C. Seismic retrofit of reinforced concrete frame buildings with hysteretic bracing systems: Design procedure and behaviour factor. *Shock. Vib.* **2017**, *2017*, e2639361. [[CrossRef](#)]
10. Nuzzo, I.; Losanno, D.; Caterino, N. Seismic design and retrofit of frames structures with hysteretic dampers: A simplified displacement-based procedure. *Bull. Earthq. Eng.* **2019**, *17*, 2787–2819. [[CrossRef](#)]
11. Bruschi, E.; Quaglini, V.; Calvi, P.M. A simplified design procedure for seismic upgrade of frame structures equipped with hysteretic dampers. *Eng. Struct.* **2021**, *251*, e113504. [[CrossRef](#)]

12. Bruschi, E. Seismic Retrofit of RC Framed Buildings with Supplementary Energy Dissipation: Modelling and Application of a Novel Lead Damper. Ph.D. Thesis, Politecnico di Milano, Milan, Italy, 2021.
13. Quaglini, V.; Pettorruso, C.; Bruschi, E. Experimental and numerical assessment of prestressed lead extrusion dampers. *Int. J. Earthq. Eng.* **2021**, *XXXVIII*, 46–69.
14. Quaglini, V.; Bruschi, E. Controllo passivo mediante controventi dissipativi. Principi generali, requisiti normativi ed evoluzione dei principali dispositivi a comportamento dipendente dallo spostamento. *Structural* **2022**, *240*, 09. [[CrossRef](#)]
15. Freddi, F.; Tubaldi, E.; Ragni, L.; Dall'Asta, A. Probabilistic performance assessment of low-ductility reinforced concrete frames retrofitted with dissipative braces. *Earthq. Eng. Struct. Dyn.* **2013**, *42*, 993–1011. [[CrossRef](#)]
16. Freddi, F.; Ghosh, J.; Kotoky, N.; Raghunandan, M. Device uncertainty propagation in low-ductility RC frame retrofitted with BRBs for seismic risk mitigation. *Earthq. Eng. Struct. Dyn.* **2021**, *50*, 2488–2509. [[CrossRef](#)]
17. American Institute of Steel Construction. *Seismic Provisions for Structural Steel Buildings*; ANSI/AISC 341-16, ANSI/AISC 341-16; American Institute of Steel Construction: Chicago, IL, USA, 2016.
18. American Society of Civil Engineers. *Minimum Design Loads and Associated Criteria for Buildings and Other Structures*; ASCE/SEI 7-16; American Society of Civil Engineers: Reston, VA, USA, 2017. [[CrossRef](#)]
19. *EN 1993-1-1*; Design of Steel Structures—Part 1-1: General Rules and Rules for Buildings. European Committee for Standardization: Brussels, Belgium, 2005.
20. *EN 1998-1*; Design of Structures for Earthquake Resistance—Part 1: General Rules, Seismic Actions and Rules for Building. European Committee for Standardization: Brussels, Belgium, 2005.
21. Tartaglia, R.; D'Aniello, M.; Landolfo, R. Numerical simulation to predict the seismic performance of a 2-story steel moment-resisting frame. *Materials* **2020**, *13*, 4831. [[CrossRef](#)]
22. Reinhorn, A.M. *The Northridge, California Earthquake of January 17, 1994: General Reconnaissance Report*; Report No. NCEER-94-0005; National Centre for Earthquake Engineering Research: Buffalo, NY, USA, 1994.
23. Youssef, N.F.G.; Bonowitz, D.; Gross, J.L. *A Survey of Steel Moment-Resisting Frame Buildings Affected by the 1994 Northridge Earthquake*; Report No. NISTR 56254; National Institute for Science and Technology: Gaithersburg, MD, USA, 1995.
24. Watanabe, E.; Sugiura, K.; Nagata, K.; Kitane, Y. Performances and damages to steel structures during 1995 Hyogoken-Nanbu earthquake. *Eng. Struct.* **1998**, *20*, 282–290. [[CrossRef](#)]
25. Federal Emergency Management Agency. *State of the Art Report on Past Performance of Steel Moment-Frame Buildings in Earthquakes*; FEMA 355E; Federal Emergency Management Agency: Washington, DC, USA, 2000.
26. Di Sarno, L.; Paolacci, F.; Sextos, A.G. Seismic performance assessment of existing steel buildings: A case study. *Key Eng. Mater.* **2018**, *763*, 1067–1076. [[CrossRef](#)]
27. Di Sarno, L.; Freddi, F.; D'Aniello, M.; Kwon, O.S.; Wu, J.R.; Gutierrez-Urzua, F.; Landolfo, R.; Park, J.; Palios, X.; Strepelias, E. Assessment of existing steel frames: Numerical study, pseudo-dynamic testing and influence of masonry infills. *J. Constr. Steel Res.* **2021**, *185*, 106873. [[CrossRef](#)]
28. Gutiérrez-Urzúa, F.; Freddi, F.; Di Sarno, L. Comparative analysis of code-based approaches for seismic assessment of existing steel moment resisting frames. *J. Constr. Steel Res.* **2021**, *181*, 106589. [[CrossRef](#)]
29. Güneysi, E.M. Seismic reliability of steel moment resisting framed buildings retrofitted with buckling restrained braces. *Earthq. Eng. Struct. Dyn.* **2012**, *41*, 853–874. [[CrossRef](#)]
30. Sorace, S.; Terenzi, G. Fluid viscous damper-based seismic retrofit strategies of steel structures: General concepts and design applications. *Adv. Steel Constr.* **2009**, *5*, 322–339.
31. Mazza, F.; Vulcano, A. Control of the earthquake and wind dynamic response of steel-framed buildings by using additional braces and/or viscoelastic dampers. *Earthq. Eng. Struct. Dyn.* **2011**, *40*, 155–174. [[CrossRef](#)]
32. Ismail, M. Seismic retrofit of steel frame structures. *Int. J. Eng. Inf. Sci.* **2020**, *15*, 106–117. [[CrossRef](#)]
33. Gutiérrez-Urzúa, F.; Freddi, F. Influence of the design objectives on the seismic performance of steel moment resisting frames retrofitted with buckling restrained braces. *Earthq. Eng. Struct. Dyn.* **2022**, *51*, 3131–3153. [[CrossRef](#)]
34. Freddi, F.; Tubaldi, E.; Zona, A.; Dall'Asta, A. Seismic performance of dual systems coupling moment-resisting and buckling-restrained braced frames. *Earthq. Eng. Struct. Dyn.* **2021**, *50*, 329–353. [[CrossRef](#)]
35. INNOSEIS. European Commission Research Programme of the Research Fund for Coal and Steel. Valorization of Innovative Anti-Seismic Devices. Work Package 4—Deliverable 4.3: Volume on Case Studies for Upgrading Existing Buildings. Available online: http://innoseis.ntua.gr/deliverables/INNOSEIS_D4.2_MidHighRiseCaseStudies.pdf (accessed on 6 June 2022).
36. Kim, J.; Choi, H. Displacement-Based Design of supplemental dampers for seismic retrofit of a framed structure. *J. Struct. Eng.* **2006**, *132*, 873–883. [[CrossRef](#)]
37. Lavan, O.; Dargush, G.F. Multi-objective evolutionary seismic design with passive energy dissipation systems. *J. Earthq. Eng.* **2009**, *13*, 758–790. [[CrossRef](#)]
38. Mazza, F.; Vulcano, A. Design of hysteretic damped braces to improve the seismic performance of steel and R.C. framed structures. *Int. J. Earthq. Eng.* **2014**, *XXXI*, 5–16.
39. Ragni, L.; Zona, A.; Dall'Asta, A. Analytical expressions for preliminary design of dissipative bracing systems in steel frames. *J. Constr. Steel Res.* **2011**, *67*, 102–113. [[CrossRef](#)]
40. Xie, Q. State of the art of buckling-restrained braces in Asia. *J. Constr. Steel Res.* **2005**, *61*, 727–748. [[CrossRef](#)]

41. Freddi, F.; Galasso, C.; Cremen, G.; Dall'Asta, A.; Di Sarno, L.; Giaralis, A.; Gutiérrez-Urzuá, F.; Málaga-Chuquitaype, F.; Mitoulis, S.A.; Petrone, C.; et al. Innovations in earthquake risk reduction for resilience: Recent advances and challenges. *Int. J. Disaster Risk Reduct.* **2021**, *60*, 102267. [CrossRef]
42. Tremblay, R.; Poncet, L.; Bolduc, P.; Neville, R.; DeVall, R. Testing and design of buckling restrained braces for canadian application. In Proceedings of the 13th World Conference in Earthquake Engineering 2004, Vancouver, BC, Canada, 1–6 August 2004; p. 200.
43. Maley, T.J.; Sullivan, T.J.; Della Corte, G. Development of a displacement-based design method for steel dual systems with buckling-restrained braces and moment-resisting frames. *J. Earthq. Eng.* **2010**, *14*, 106–140. [CrossRef]
44. Kalapodis, N.A.; Mucho, E.V.; Beskos, D.E. Seismic design of plane steel MRFs, EBFS and BRBFS by improved direct displacement-based design method. *Soil Dyn. Earthq. Eng.* **2022**, *153*, 107111. [CrossRef]
45. Ferraioli, M.; Lavino, A. A Displacement-Based Design Method for seismic retrofit of RC buildings using dissipative braces. *Math. Probl. Eng.* **2018**, 5364564, 28. [CrossRef]
46. Kim, J.; Seo, Y. Seismic design of low-rise steel frames with buckling-restrained braces. *Eng. Struct.* **2004**, *26*, 543–551. [CrossRef]
47. Quaglino, V.; Bruschi, E.; Pettorruso, C. Dimensionamento di dispositivi dissipativi per la riabilitazione sismica di strutture intelaiate. *Structural* **2021**, 237. paper 25. [CrossRef]
48. Bruschi, E.; Quaglino, V.; Calvi, P.M. A simplified design procedure to improve the seismic performance of RC framed buildings with hysteretic damped braces. In Proceedings of the New Metropolitan Perspectives 2022—5th International Symposium “Post COVID Dynamics: Green and Digital Transition, between Metropolitan and Return to Villages’ Perspectives”, Reggio Calabria, Italy, 25–27 May 2022; Calabrò, F., Della Spina, F., Piñeira Mantiñán, M.J., Eds.; Springer: Reggio Calabria, Italy, 2022; Volume 482, pp. 2173–2182, ISBN 978-3-031-06825-6.
49. ATC-40; Seismic Evaluation and Retrofit of Concrete Buildings. Applied Technology Council: Redwood City, CA, USA, 1996.
50. Fajfar, P. Capacity spectrum method based on inelastic demand spectra. *Earthq. Eng. Struct. Dyn.* **1999**, *28*, 979–993. [CrossRef]
51. Italian Council of Public Works. *Technical Standards on Constructions*; Italian Council of Public Works: Rome, Italy, 2018. (In Italian)
52. Italian Council of Public Works. *Commentary on the Technical Standards on Constructions*; Italian Council of Public Works: Rome, Italy, 2019. (In Italian)
53. EN 1998-3; Design of Structures for Earthquake Resistance—Part 3: Assessment and Retrofitting of Buildings. European Committee for Standardization: Brussels, Belgium, 2005.
54. Vamvatsikos, D.; Bakalis, K.; Kohrangi, M.; Pyrza, S.; Castiglioni, C.A.; Kanyilmaz, A.; Morelli, F.; Stratan, A.; D’Aniello, M.; Calado, L.; et al. A risk-consistent approach to determine EN1998 behaviour factors for lateral load resisting systems. *Soil Dyn. Earthq. Eng.* **2020**, *131*, 106008. [CrossRef]
55. De Domenico, D.; Gandelli, E.; Quaglino, V. Cyclic engagement of hysteretic steel dampers in braced buildings: A parametric investigation. *Bull. Earthq. Eng.* **2021**, *19*, 5219–5251. [CrossRef]
56. McKenna, F.; Fenves, G.I.; Scott, M.H. *Open System for Earthquake Engineering Simulation*; Pacific Earthquake Engineering Research Center: Berkeley, CA, USA, 2000.
57. OpenSeesWiki Online Manual. Available online: https://opensees.berkeley.edu/wiki/index.php/Main_Page (accessed on 9 April 2022).
58. Bosco, M.; Tirca, L. Numerical simulation of steel I-shaped beams using a fiber-based damage accumulation model. *Constr. Steel Res.* **2017**, *133*, 241–255. [CrossRef]
59. Ribeiro, F.L.; Barbosa, A.R.; Scott, M.H.; Neves, L.C. Deterioration modeling of steel moment-resisting frames using finite-length plastic hinge force based beam column elements. *J. Struct. Eng.* **2015**, *141*, e04014112. [CrossRef]
60. Bruschi, E.; Calvi, P.M.; Quaglino, V. Concentrated plasticity modelling of RC frames in time-history analyses. *Eng. Struct.* **2021**, *243*, e112716. [CrossRef]
61. Ferraioli, M. Evaluation of dynamic increase factor in progressive collapse analysis of steel frame structures considering catenary action. *Steel Comp. Struct.* **2019**, *30*, 253–269. [CrossRef]
62. Mohebi, B.; Chegini, A.H.; Miri, A.R. A new damage index for steel MRFs based on incremental dynamic analysis. *J. Constr. Steel Res.* **2019**, *156*, 137–154. [CrossRef]
63. Pandikkadavath, M.S.; Shaijal, K.M.; Mangalathu, S.; Davis, R. Seismic robustness assessment of steel moment resisting frames employing material uncertainty incorporated incremental dynamic analysis. *J. Constr. Steel Res.* **2022**, *191*, e107200. [CrossRef]
64. Guan, X.; Burton, H.; Shokrabadi, M. A database of seismic design nonlinear models, and seismic responses for steel moment resisting frame buildings. *Earthq. Spectra* **2021**, *37*, 1199–1222. [CrossRef]
65. Ibarra, L.F.; Medina, R.A.; Krawinkler, H. Hysteretic models that incorporate strength and stiffness deterioration. *Earthq. Eng. Struct. Dyn.* **2005**, *34*, 1489–1511. [CrossRef]
66. Chopra, A.K.; McKenna, F. Modeling viscous damping in nonlinear response history analysis of buildings for earthquake excitation. *Earthq. Eng. Struct. Dyn.* **2016**, *45*, 193–211. [CrossRef]
67. Ferraioli, M. Multi-mode pushover procedure for deformation demand estimates of steel moment-resisting frames. *Int. J. Steel Struct.* **2017**, *17*, 653–676. [CrossRef]
68. Jin, S.; Du, H.; Bai, J. Seismic performance assessment of steel frame structures equipped with buckling-restrained slotted steel plate shear walls. *J. Constr. Steel Res.* **2021**, *182*, e106699. [CrossRef]
69. Mirjalili, M.R.; Rofooei, F.R. The modified dynamic-based pushover analysis of steel moment resisting frames. *Struct. Des. Tall Spec. Build.* **2017**, *26*, e1378. [CrossRef]

70. Di Sarno, L.; Wu, J.R. Fragility assessment of existing low-rise steel moment-resisting frames with masonry infills under mainshock-aftershock earthquake sequences. *Bull. Earthq. Eng.* **2021**, *19*, 2483–2504. [[CrossRef](#)]
71. Scott, M.H.; Fenves, G.L. Plastic hinge integration methods for force-based beam-column elements. *J. Struct. Eng.* **2006**, *132*, 244–252. [[CrossRef](#)]
72. Lignos, D.G.; Krawinkler, H. Development and utilization of structural component databases for performance-based earthquake engineering. *J. Struct. Eng.* **2013**, *139*, 1382–1394. [[CrossRef](#)]
73. Gioncu, V.; Pecteu, D. Available rotation capacity of wide-flange beams and beam-columns Part 1. Theoretical approaches. *J. Constr. Steel Res.* **1997**, *43*, 161–217. [[CrossRef](#)]
74. Menegotto, M.; Pinto, P.E. Method of analysis for cyclically loaded RC plane frames including changes in geometry and non-elastic behaviour of elements under combined normal force and bending. In Proceedings of the IABSE Symposium on Resistance and Ultimate Deformability of Structures Acted on by Well Defined Repeated Loads, Lisbon, Portugal; 1973; Volume 11, pp. 15–22.
75. Barbagallo, F.; Bosco, M.; Ghersi, A.; Marino, E.M.; Rossi, P.P. Seismic assessment of steel MRFs by cyclic pushover analysis. *Open Constr. Build. Tech. J.* **2019**, *13*, 12–26. [[CrossRef](#)]
76. EN 1990; Basis of Structural Design. Eurocode 1. European Committee for Standardization: Brussels, Belgium, 2005.
77. Barbagallo, F.; Bosco, M.; Marino, E.M.; Rossi, P.P. Seismic design and performance of dual structures with BRBs and semi-rigid connections. *J. Constr. Steel Res.* **2019**, *158*, 306–316. [[CrossRef](#)]
78. Barbagallo, F.; Bosco, M.; Marino, E.M.; Rossi, P.P. Achieving a more effective concentric braced frame by the double-stage yield BRB. *Eng. Struct.* **2019**, *186*, 484–497. [[CrossRef](#)]
79. Uriz, P.; Mahin, S.A. *Toward Earthquake-Resistant Design of Concentrically Braced Steel-Frame Structures*; PEER Report 2008/08; Pacific Earthquake Engineering Research Center: Berkeley, CA, USA, 2008.
80. Xuewei, C.; Xiaolei, H.; Cheang, J.; Shengyi, L.; Guiniu, M. Dynamic inelastic numerical simulation for a shaking table test of a full scale steel moment frame structure based on OpenSEES. In Proceedings of the 14th World Conference on Earthquake Engineering, Beijing, China, 12–17 October 2008.
81. Filippou, F.C.; Popov, E.P.; Bertero, V.V. *Effects of Bond Deterioration on Hysteretic Behavior of Reinforced Concrete Joints*; Report EERC 83-19; Earthquake Engineering Research Center: Berkeley, CA, USA, 1983.
82. Priestley, M.J.N.; Calvi, G.M.; Kowalsky, M. *Displacement-Based Seismic Design of Structures*; IUSS Press: Pavia, Italy, 2007.
83. Sullivan, T.; Maley, T.; Calvi, G.M. Seismic response of steel moment resisting frames designed using a Direct DBD procedure. In Proceedings of the 8th International Conference on Structural Dynamics, EURO DYN 2011, Leuven, Belgium, 4–6 July 2011.
84. Keykhosravi, A.; Aghayari, R. Evaluating response modification factor (R) of reinforced concrete frames with chevron brace equipped with steel slit damper. *KSCE J. Civil. Eng.* **2017**, *21*, 1417–1423. [[CrossRef](#)]
85. Fahiminia, M.; Ghaderi, M.R.; Zahrai, S.M. Seismic performance of chevron braced frames with shape memory alloy vertical shear link. *Struct. Des. Tall. Spec. Build.* **2019**, *28*, e1658. [[CrossRef](#)]
86. Sullivan, T.J.; Lago, A. Towards a simplified Direct DBD procedure for the seismic design of moment resisting frames with viscous dampers. *Eng. Struct.* **2012**, *35*, 140–148. [[CrossRef](#)]
87. Sullivan, T.J. Direct displacement-base seismic design of steel eccentrically braced frame structures. *Bull. Earthq. Eng.* **2013**, *11*, 2197–2231. [[CrossRef](#)]
88. Ponzio, F.C.; Di Cesare, A.; Telesca, A.; Pavese, A.A.; Furinghetti, M. Advanced modelling and risk analysis of RC buildings with sliding isolation systems designed by the Italian Seismic Code. *Appl. Sci.* **2021**, *11*, 1938. [[CrossRef](#)]
89. Gandelli, E.; Taras, A.; Distl, J.; Quaglini, V. Seismic retrofit of hospitals by means of hysteretic braces: Influence on acceleration-sensitive non-structural components. *Front. Built. Environ.* **2019**, *5*, e100. [[CrossRef](#)]
90. Scozzese, F.; Gioiella, L.; Dall’Asta, A.; Ragni, L.; Tubaldi, E. Influence of viscous dampers ultimate capacity on the seismic reliability of building structures. *Struct. Saf.* **2021**, *91*, e102096. [[CrossRef](#)]
91. Castaldo, P.; Tubaldi, E.; Selvi, F.; Gioiella, L. Seismic performance of an existing RC structure retrofitted with buckling restrained braces. *J. Build. Eng.* **2021**, *33*, 101688. [[CrossRef](#)]
92. Greco, A.; Caddemi, S.; Calì, I.; Fiore, I. A Review of Simplified Numerical Beam-like Models of Multi-Storey Framed Buildings. *Buildings* **2022**, *12*, 1397. [[CrossRef](#)]
93. SIMQKE (SIMulation of Earthquake Ground Motions). Available online: https://gelfi.unibs.it/software/simqke/simqke_gr.htm (accessed on 10 July 2022).
94. Bruschi, E.; Quaglini, V. Assessment of a novel hysteretic friction damper for the seismic retrofit of reinforced concrete frame structures. *Structures* **2022**, *46*, 793–811. [[CrossRef](#)]
95. Bungale, S.T. *Wind and Earthquake Resistant Buildings Structural Analysis and Design*, 1st ed.; Marcel Dekker: New York, NY, USA, 2005; ISBN 978-04-2909-603-7.
96. MacRae, G.A.; Urmson, C.R.; Walpole, W.R.; Moss, P.; Hyde, K.; Clifton, C. Axial shortening of steel columns in buildings subjected to earthquakes. *Bull. N. Z. Soc. Earthq. Eng.* **2009**, *42*, 275–287. [[CrossRef](#)]

Disclaimer/Publisher’s Note: The statements, opinions and data contained in all publications are solely those of the individual author(s) and contributor(s) and not of MDPI and/or the editor(s). MDPI and/or the editor(s) disclaim responsibility for any injury to people or property resulting from any ideas, methods, instructions or products referred to in the content.